Analysis of the Operating Mechanism of Photovoltaic Power Generation Systems Constrained by Arc Faults and Its Identification Methods

Kailong CHEN, Jiaxun TENG, Peiyi LI, Junjie GUO, Lei QI, and Xiaofeng SUN

***Abstract*—Series/parallel arc faults are typical problems existing between photovoltaic (PV) and boost converter. Current research lacks a unified system model to describe the operation mechanism and power characteristics under arc faults. This paper proposes an equivalent model of PV-boost power generation system based on series/parallel arc constraints. Firstly, by coupling the arc equivalent model in the PV model, the output characteristics of the PV system in normal and fault states are obtained. Then, by adding the arc link in the power conversion and control model of the PV-boost system, the operation mechanism and power transfer characteristics of the system under two types of arc faults are revealed. Finally, based on the multi-modal PV output voltage-current characteristics under arc faults and the voltage-current characteristics at the input end of the boost under maximum power point tracking control, a specific fault identification and classification method for series/parallel arcs is designed, which is easy to implement in engineering and based on the degree of hazard. The feasibility of this scheme is verified.**

***Index Terms*—Arc model, boost, identification, mechanism, photovoltaic.**

I. Introduction

PHOTOVOLATIC power generation has become one of the key technologies promoting the low-carbon transformation of energy due to its advantages such as no pollution, no noise, and flexible distributed deployment [1], [2]. The centralized architecture of PV power station adopts a modular series-parallel approach to form a PV array, and realizes DC-AC power conversion and grid connection through grid-connected inverters. The structure is simple and the inverter efficiency is relatively high, but the system expansion and redundancy capabilities are poor [3].

The multi-branch architecture is equipped with independent DC-DC converter in each branch of the PV array. This topology effectively enhances the output power and operational flexibility of the PV grid-connected system. Even when a single DC/DC converter fails, the system can still operate stably. However, it has problems such as rising hardware costs and the persistence of series faults of PV modules [4].

With the rapid development of PV power generation systems towards large capacity and high voltage, the problem of fault protection on the DC side has become increasingly prominent. Especially DC arc faults, due to their strong concealment, high randomness and difficulty in self-extinguishing, have become the primary hidden danger threatening the safe operation of PV systems [5], [6]. According to the analysis of fault mechanisms, DC arc faults are mainly divided into series arc faults and parallel arc faults. Parallel arcs are usually caused by insulation breakdown due to aging of wires or equipment [7], [8]. Series faults are induced by poor contact, aging of lines, or environmental factors, and their fault characteristics are more complex and occur more frequently [9], [10]. Scholars have conducted in-depth research in the fields of DC arc fault mechanism, fault detection and fault protection.

The occurrence mechanism of arc is the basis for further theoretical analysis [11], [12] and simulation tests [13], [14]. Regarding the mechanism research of DC arc, literature [11] established an arc fault model for PV systems, systematically analyzed the fault generation mechanism, and analyzed the DC characteristics based on the voltage and current waveform features. [12] discussed the use of actual data recorded in the PV system to drive an effective DC series arc model from the original Nottingham arc model. This model has three parameters, including a current index constant, model order, and two time series coefficients. [13] proposed a heuristic average model based on the principle of arc power balance and provided a current-controlled arc noise simulation method based on the correlation mechanism between arc noise and arc current. By superimposing arc noise on the proposed average model, the dynamic characteristics of DC series arc can be accurately described. [14] modeled the physical characteristics of arcs in photovoltaic (PV) systems. The simulations were carried out with ANSYS Fluent and ANSYS Maxwell in the ANSYS software. The results contributed to the standardization

Manuscript received July 23, 2025; revised November 24, 2025 and December 31, 2025; accepted January 27, 2026. Date of publication March 30, 2026; date of current version March 11, 2026. (*Corresponding author: Jiaxun Teng.*)

K. Chen and P. Li are both with the Guodian Nanjing Automation Co., Ltd., Nanjing 211100, China (e-mail: chenkailong@chd.com.cn; lipeiyi@chd.com.cn).

J. Teng, J. Guo, L. Qi, and X. Sun are with the Department of Electronics Engineering, Yanshan University, Qinhuangdao 066004, China (e-mail: tengjiaxun@ysu.edu.cn; 2320169791@qq.com; qil@ysu.edu.cn; sxf@ysu.edu.cn).

Digital Object Identifier 10.24295/CPSSTPEA.2026.00001

model for risk assessment of DC devices.

For the detection and protection of DC arc faults, the main approaches can be classified into those based on hardware circuits, mathematical models, and artificial intelligence.

In the hardware circuit approach, [15]–[17] studied the modeling, detection, and protection strategies of DC arc signals for a four-switch buck-boost circuit by leveraging the combination of switch states of the four switches and the current characteristics of the intermediate inductor. However, this method is only applicable to specific type of converter. [18] added a resonant filter circuit at the input stage of the DC/DC converter to decouple the arc fault signal between the filter and the converter, thereby enabling fault detection through current sampling of the resonant filter. This method accurately detects DC arc faults but at the cost of additional passive components and sensors.

In the mathematical model approach, [19] and [20] conducted comparative studies on the frequency domain characteristics of PV arc fault signals using Fourier transform and wavelet transform, respectively. The results show that wavelet analysis is more suitable for the frequency domain feature analysis of this type of signal. [21] developed a DC system arc fault detection technology based on modeling and integral residual analysis by establishing generalized state-space average models of the DC system under normal operation and arc fault conditions. [22] proposed a hybrid DC arc current model based on time series interval prediction and equivalent circuit model. The relationship between arc current and electrode separation speed, arc gap length, voltage and current levels was studied.

In artificial intelligence method, the data-driven approach is mainly adopted. [23] proposed a DC series arc fault detection and arc quenching method combining current modulation with machine learning, which improved the accuracy of fault detection through double screening. [24] presented an arc detection neural network based on a time convolutional network to extract current waveform features, using the performance of arcs in typical frequency bands as the detection basis. [25] conducted a comprehensive analysis of the series arc fault detection technology in PV systems based on artificial intelligence, discussing key challenges and future directions such as hybrid models, transfer learning, and implementation in resource-constrained edge devices. [26], through a comprehensive comparative analysis of artificial intelligence-based and model-based methods, and supported by a thorough literature review and experimental verification, summarized the advantages and disadvantages of these two methods.

Regarding the issues of series and parallel arcs in PV-boost systems, this paper investigates the underlying mechanisms and establishes a unified mathematical model to characterize the input-side voltage and current behavior of boost converter. Based on this model, an engineering-practical arc detection method is proposed. The main contributions are as follows:

1) A unified modeling framework for the PV-arc-boost system is developed based on arc constraints. The existing studies have only been based on the model of a single arc. The proposed unified model can explain the interaction mechanism of PV-arc-boost under different arc types.

2) An easily implementable detection method is proposed. Existing frequency-domain models and artificial intelligence-based approaches often entail high computational complexity, making them unsuitable for distributed PV-boost control systems. In contrast, the threshold-based detection method requires significantly lower computational resources, enabling practical deployment in real-time applications.

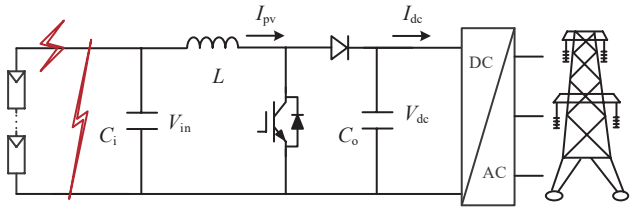

Fig. 1. The typical PV power generation unit system.

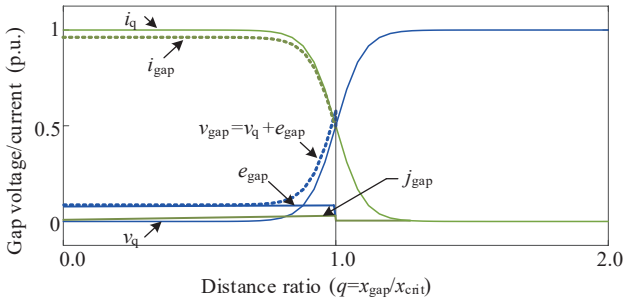

Fig. 2. Curves of arc voltage and current.

II. Analysis of DC Arc Faults in PV Systems

The typical PV power generation unit system is shown in Fig. 1. The PV power generation unit takes the boost circuit as the main topology, with PV as the input. The output end is usually a voltage source type load, which represents the equivalent load of the primary and secondary combiner boxes connected to the rear stage of the power generation unit.

In the research on DC arc fault models, the conventional approach is to obtain the time-domain data information of DC arcs through experiments, and then study their volt-ampere characteristics. The volt-ampere characteristic model reflecting DC fault arcs is obtained through data fitting methods. Fig. 2 shows a model diagram of the arc volt-ampere characteristics approximated by hyperbolic functions to characterize the arc voltage and current. Among them, the horizontal q-axis represents the distance ratio, $q = x_{gap}/x_{crit}$, where x_{gap} is the distance between the two poles at the point where the arc occurs, and x_{crit} is the limit distance between the two poles to reach the arc extinction condition. v_{gap} and i_{gap} represent the voltage and current of the fault gap. v_q and i_q represent the hyperbolic models of voltage and current in the fault gap. e_{gap} and j_{gap} represent the equivalent electromotive force of the arc and its response current. The simulation of arc characteristics based on trigonometric function curves is a typical method in existing research. On the basis of the existing research ideas

[27], [28], this paper further conducts modeling and analysis by combining the fluctuations introduced on the bus between PV-boost due to power control.

1) Fault gap voltage model:

Referring to Fig. 2, v_{gap} can be decomposed into a nonlinear hyperbolic tangent function voltage v_q and an equivalent electromotive force e_{gap} of the arc when $0 < q < 1$. Among them, the hyperbolic tangent function voltage v_q is

$$\begin{aligned} v_q &= (V_s + \Delta V_{dc})\{1/2 + \tanh[a(q-1)]/2\} \\ &= (V_s + \Delta V_{dc})\left(\frac{e^{2qa}}{e^{2a} + e^{2qa}}\right) \end{aligned} \tag{1}$$

Among them, V_{dc} is the average DC voltage before the fault, ΔV_{dc} is the bus fluctuation voltage (on the PV side, it is the fluctuation caused by maximum power point tracking (MPPT) regulation, and on the bus side, it is the fluctuation generated by the inverter regulation of the subsequent stage), and α is a variable that controls the slope of v_q. The equivalent electromotive force e_{gap} can be approximated by an approximate rectangular pulse with an amplitude of $a + bx_{gap}$, and its expression is

$$e_{gap} = \frac{1}{2}(a + bx_{gap})\{\tanh(\lambda q) - \tanh[\lambda(q-1)]\} \tag{2}$$

Among them, λ controls the rate at which e_{gap} rises and falls. A relatively effective value is $\lambda = 100$, but other values can also be used. It should be noted that e_{gap} initially dominates, but when the arc approaches extinction, v_q takes the lead.

2) Fault gap current model:

Similar to the gap voltage, the gap current i_{gap} can also be decomposed into the nonlinear hyperbolic tangent function current i_q and the response current of the equivalent step electromotive force e_{gap} of the arc. Among them, the hyperbolic tangent function current i_q:

$$i_q = I_{load}\left\{\frac{1}{2} - \frac{1}{2}\tanh[a(q-1)]\right\} = I_{load}\Big/\left[1 + e^{2a(q-1)}\right] \tag{3}$$

Among them, I_{load} is the average DC current before failure, and j_{gap} is the system's response to e_{gap}, which can be approximately expressed as

$$j_{gap} = \frac{e_{gap}}{(R_{gap} + R_{load} + R_g)} \approx \frac{e_{gap} I_{load}}{V_s} \tag{4}$$

In the above formula, R_{gap} represents the gap resistance and can be disregarded in the range of $0 < q < 1$. R_g is the internal resistance of the system and is very small compared to R_{load}. The dominant resistance in the denominator is R_{load}, which $=V_{dc}/I_{load}$. This value can be known before a fault occurs.

3) Fault gap resistance model:

The synchronous changes of arc voltage and current in Figs. 1 and 2 indicate that the arc impedance is resistive. The arc fault model is shown in Fig. 3. Although the ratio $R_{gap}=v_q/i_{gap}$ can approximate the gap resistance relatively well, it will produce an unnecessary complex and lengthy expression. Researcher has found that the influence of j_{gap} on R_{gap} is negligible, and thus a much simpler R_{gap} expression can be obtained without significantly losing accuracy. The simplified expression of R_{gap} is:

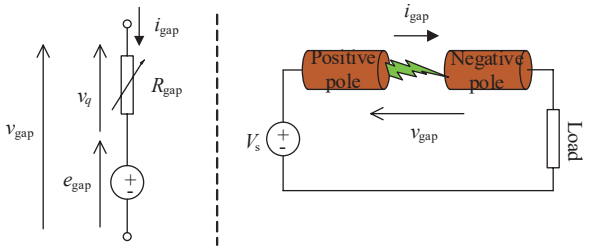

Fig. 3. Arc fault model.

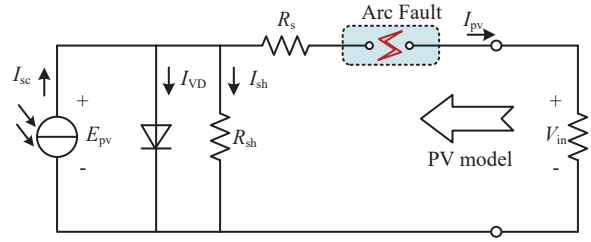

Fig. 4. Equivalent model of PV series arc.

$$R_{gap} = \frac{v_q}{i_{gap}} = \frac{v_q}{i_q - j_{gap}} \approx \frac{V_{dc}}{I_{load}} e^{2a(q-1)}\Omega \tag{5}$$

In the above formula, the value of a can be determined in the following way: assuming the resistance value when the electrode is closed ($q = 0$) is R_{closed}, then it can obtain as:

$$R_{gap|q=0} = \frac{V_s}{I_{load}} e^{-2a} = R_{closed}\Omega \tag{6}$$

$$a = -\frac{1}{2}\ln\left(\frac{R_{closed} I_{load}}{V_{dc}}\right) \tag{7}$$

III. Unified Model of PV-Series Arc-Boost and Its Performance

A. Analysis of External Characteristics of PV Series Arcs

The equivalent model of the PV generator is shown in Fig. 4, where I_{sc} represents the current excited by photons in the PV cell, and its value depends on the degree of light, the area of the PV panel and the temperature, and E_{pv} is its equivalent electromotive force. I_{VD} is the current passing through the PN junction of a PV cell, and its magnitude is related to the electromotive force and temperature of the PV cell. R_{sh} and R_s represent the equivalent parallel and series resistances of PV cells.

The diode current I_{VD} is the total diffusion current through

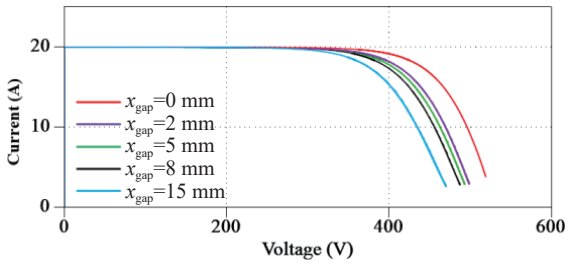

Fig. 5. The external characteristic curve of PV series arc.

the PN junction, and its expression can be obtained from existing research [29]:

$$I_{VD} = I_{D0}(e^{\frac{qE}{AKT}} - 1) \tag{8}$$

I_{D0} is the saturation current in the absence of light. q is the charge of an electron,1.6×10^{-19} °C; K is the Boltzmann constant, 1.38×10^{-23} J/K; A is a constant factor (1 when the forward bias voltage is large and 2 when it is small), and further, the load current can be obtained as:

$$I_{pv} = I_{sc} - I_{D0}(e^{\frac{q(V_{in}+I_{pv}R_s)}{AKT}} - 1) - \frac{V_{in}+I_{pv}R_s}{R_{sh}} \tag{9}$$

After considering the parameters of the PV cell and the external environment, the *I-V* curve can be calculated from short-circuit V_{in}= 0 to open-circuit V_{in}=V_{oc} according to the above formula.

As shown in Fig. 4, when a series arc fault occurs on the PV busbar, it can be observed from the input port of the PV converter that the arc impedance is bound to affect the overall external characteristics of the PV. The external characteristics of PV cells under arc faults can be obtained from (2), (5) and (9):

$$I_{pv} = I_{sc} - I_{D0}[e^{\frac{q(V_{in}+I_{pv}R_s+I_{pv}R_{gap}+e_{gap})}{AKT}} - 1] - \frac{V_{in}+I_{pv}R_s+I_{pv}R_{gap}+e_{gap}}{R_{sh}} \tag{10}$$

As shown in Fig. 5, it is the *I-V* curve of the external characteristic test under the PV series arc fault. With the increase of the distance between the two poles of the series arc, the arc impedance increases. Under the MPPT control of the PV cell, the output voltage corresponding to the same current value gradually decreases.

B. Series Arc Constraint Based System Model and Control Characteristics

When a series arc fault occurs on the PV busbar, the system equivalent average model for arc fault constraints is established as shown in Fig. 6. The output current of the series arc busbar of PV cells is the PV current I_{pv}, and the output voltage (boost input voltage) is:

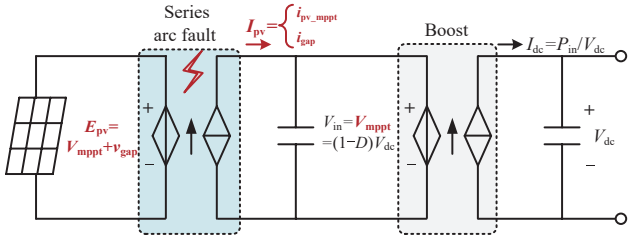

Fig. 6. Equivalent average model of the system under series arc.

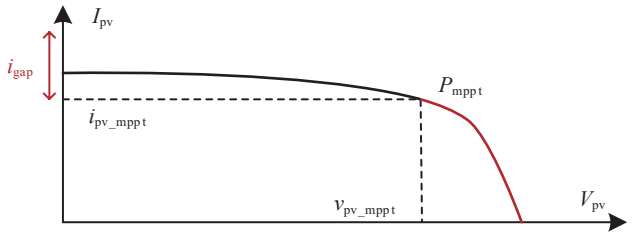

Fig. 7. The *I-V* curve of situation 1.

$$V_{in} = E_{pv} - v_{gap} \tag{11}$$

In the series arc link, the voltage and current characteristics of the arc, as well as the output characteristics of the PV cell, are comprehensively considered, and the situation is classified and explained based on the distance between the two poles of the arc.

Firstly, the distance between the two poles of the arc is defined as x_{gap}, and the transfer limit of the arc current under a fixed distance between the two poles is i_{gap}. When x_{gap}= x_1, i_{pv_mppt} = i_{gap}; when $x_{gap} \geqslant x_2$, the arc is extinguished.

1) Situation 1: When $0 < x_{gap} \leqslant x_1$, $i_{pv\_mppt} \leqslant i_{gap}$

The *I-V* curve of situation 1 is shown in Fig. 7.

Current characteristic: The MPPT current of PV is less than the current transmission capacity of the arc. At this time, the output current of the PV:

$$I_{pv} = i_{pv\_mppt} \tag{12}$$

Voltage characteristics: By adjusting the MPPT control of boost, the maximum power output can be achieved. At this point, the boost input voltage control features:

$$V_{in} = V_{mppt} = E_{pv\_mppt} - v_{gap} \tag{13}$$

Power characteristics: In this case, the boost input power and the series arc loss power are respectively:

$$\begin{cases} P_{in} = V_{in}I_{pv} = V_{in}i_{pv\_mppt} \\ P_{gap\_loss} = v_{gap}i_{pv\_mppt} \end{cases} \tag{14}$$

2) Situation 2: When $x_1 < x_{gap} < x_2$, $i_{pv\_mppt} > i_{gap}$

Current characteristics: The MPPT current of PV is greater than the arc current transmission capacity, and the PV cell can no longer operate at maximum power. At this time, the bus current transmission is constrained by the arc current.

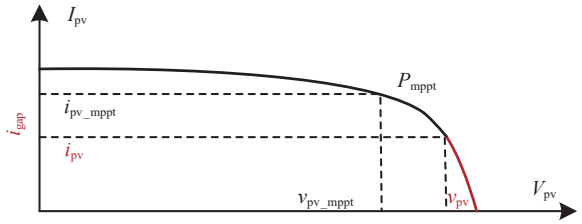

Fig. 8. The *I-V* curve of situation 2.

$$I_{pv} = i_{gap} \tag{15}$$

Voltage characteristics: When the distance between the two stages of the arc is x_{gap}, the *I-V* external characteristic curve of the PV series arc can be calculated from the model shown in (10), as shown in Fig. 8. When the arc transmission current is lower than the maximum power point current of the PV, the PV bus current is transmitted in i_{gap}. According to (10), the corresponding series arc voltage of the PV at this current is v_{pv}. At this point, the boost input voltage characteristics are:

$$V_{in} = v_{pv} = E_{pv} - v_{gap} \tag{16}$$

Power characteristics: In this case, the PV cell no longer transmits at the maximum power but outputs the power constrained by the arc current. The boost input power and the series arc loss power are respectively:

$$\begin{cases} P_{in} = V_{in} I_{pv} = v_{pv} i_{gap} \\ P_{gap\_loss} = v_{gap} i_{gap} \end{cases} \tag{17}$$

3) Situation 3: When $x_{gap} \geqslant x_2$, $i_{gap} = 0$.

In this situation, the distance between the two stages of the arc exceeds the critical value for arc ignition, the arc disappears, and the PV busbar is in an open circuit state.

IV. Unified Model of PV-Parallel Arc-Boost and Its Performance

A. Analysis of External Characteristics of PV Parallel Arcs

As shown in Fig. 9, when a parallel arc fault occurs on the PV busbar, it can be observed from the input port of the PV converter that the current branch generated by the parallel arc will affect the overall external characteristics of the PV. The external characteristics of PV cells under arc faults can be obtained from (2), (5) and (9):

$$I_{pv} = I_{sc} - I_{D0}\left[e^{\frac{q(V_{in}+I_{pv}R_s)}{AKT}} - 1\right] - \frac{V_{in} + I_{pv}R_s}{R_{sh}} - i_{gap} \tag{18}$$

As shown in Fig. 10, it is the external characteristic *I-V* curve under the PV parallel arc fault. With the reduction of the distance between the two poles of the parallel arc, the power loss increases, resulting in a gradual decrease in the output

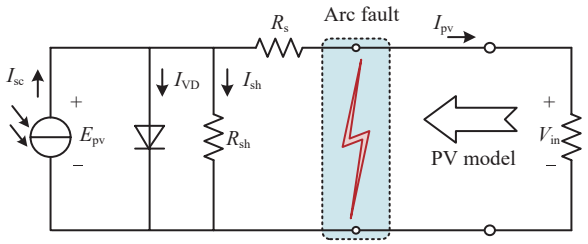

Fig. 9. Equivalent average model of the system under parallel arc.

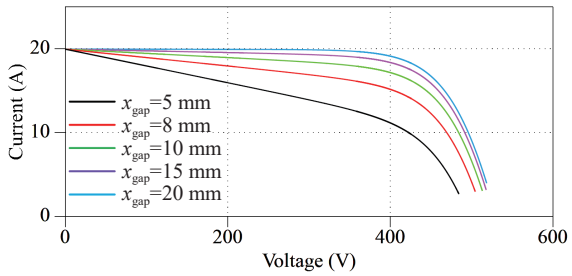

Fig. 10. The external characteristic curve of PV parallel arc.

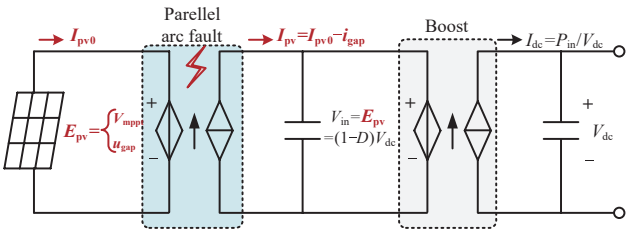

Fig. 11. Equivalent average model of the system under parallel arc.

power of the PV parallel arc system.

B. Parallel Arc Constraint Based System Model and Control Characteristics

When a parallel arc fault occurs on the PV busbar, the system equivalent average model for arc fault constraints is established as shown in Fig. 11. The output voltage (boost input voltage) of the parallel arc bus of the PV cell is E_{pv}, and the output current (boost input current) is:

$$I_{pv} = I_{pv0} - i_{gap} \tag{19}$$

In the parallel arc stage, the voltage and current characteristics of the arc, as well as the output characteristics of the PV cell, are comprehensively considered, and the situation is classified and explained based on the distance between the two poles of the arc.

Also take the distance between the two poles as the standard for different situations: when $x_{gap} = x_3$, an arc begins; When $x_{gap} = x_4$, $i_{pv\_mppt} = i_{gap}$; When $x_{gap} = x_5$, $i_{pv\_max} = i_{gap}$. The schematic diagram of the current characteristics corresponding to distance between two poles of gap is shown in Fig. 12(a). The following is a situation-by-situation discussion of the current characteristics corresponding to the distance between the two

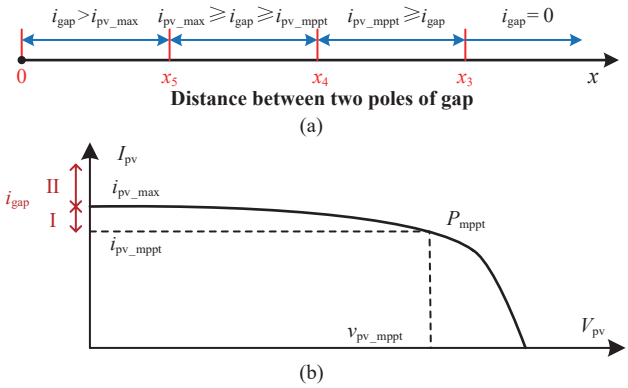

Fig. 12. (a) Schematic diagram of the current characteristics corresponding to distance between two poles of gap, (b) Situation 5 and situation 6.

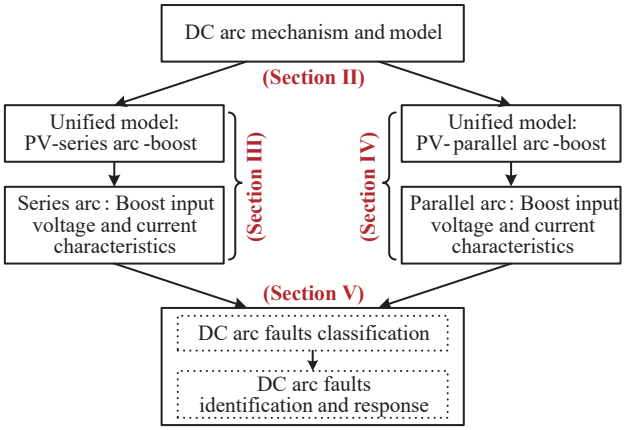

Fig. 13. Overall section logical relationship diagram.

poles of an DC arc.

As shown in Fig. 12(a), when $x_{gap} \geqslant x_3$, $i_{gap}=0$. In this situation, the distance between the two stages of the arc exceeds the critical value for arc ignition, the arc disappears, and the parallel arc branch is in an open circuit state. In this case, the output current and voltage characteristics of the PV parallel arc are consistent with those in the conventional situation, and no special explanation is required.

1) Situation 4: When $x_3>x_{gap}>x_4$, $i_{pv\_mppt}>i_{gap}$

Voltage characteristics: When a parallel arc occurs, within a certain two-stage interval range, the MPPT current of the PV is greater than the arc current transmission capacity. At this time, the PV busbar can still be controlled at the MPPT voltage through boost. At this point, the input voltage control feature of boost is:

$$V_{in}=V_{mppt} \tag{20}$$

Current characteristics: The MPPT current of the PV is greater than the current transmission capacity of the arc. When the PV cell operates in the MPPT mode, the input current of boost at this time is:

$$I_{pv}=i_{pv\_mppt}-i_{gap} \tag{21}$$

Power characteristics: In this case, the boost input power and the parallel arc loss power are respectively:

$$\begin{cases} P_{in}=V_{in}I_{pv}=V_{mppt}\left(i_{pv\_mppt}-i_{gap}\right) \\ P_{gap\_loss}=V_{mppt}i_{gap} \end{cases} \tag{22}$$

2) Situation 5: When $x_4>x_{gap}\geqslant x_5$, $i_{pv\_max}\geqslant i_{gap}\geqslant i_{pv\_mppt}$

In this case, if the PV system operates in MPPT mode, all the PV power generation will flow into the parallel arc branch. As shown in Fig. 12, when the current transmission capacity of the parallel arc is in interval I, by controlling the PV bus voltage through boost to make $I_{pv}>i_{gap}$, only a small portion of the power can be sent to boost, that is, $(I_{pv}-i_{gap})/I_{pv}$.

3) Situation 6: When $x_{gap}<x_5$, $i_{gap}>i_{pv\_max}$

When the parallel arc current transmission occurs in interval II, boost can no longer allocate power. Whether in Section I or Section II, the arc will cause relatively intense combustion, which will affect the safety of the system.

Therefore, for scenarios 5 and 6, in engineering applications, the boost switch tube as shown in Fig. 2 can be controlled in a normally closed manner. By performing a short-circuit operation on the PV panel, the output voltage of the PV cell can be reduced to nearly 0. Under this response measure, the voltage at both ends of the parallel arc can no longer maintain the combustion of the parallel arc, thereby achieving the goal of arc extinction.

V. Identification and Response to Arc Faults in PV Busbar

This article starts with the analysis of the arc mechanism (Section II), then proceeds to the PV-series arc-boost unified model based on the series arc constraint (Section III) and the PV-series arc-boost unified model based on the parallel arc constraint (Section IV), and finally to the arc fault identification scheme on the PV busbar in this section. The overall section logical relationship diagram is shown in Fig. 13.

In the previous two sections, the PV external characteristics of the series arc and parallel arc of the PV busbar and the equivalent model of the system were analyzed, and the voltage control and current transfer characteristics of the boost input terminal under various arc fault conditions were given. This section comprehensively examines the voltage-current characteristics of PV output under multiple conditions of arc faults and the voltage-current features of the boost input terminal under maximum power tracking control to conduct specific fault identification and classification of series/parallel arcs based on the degree of hazard.

A. Identification and Response Algorithm

Unlike the traditional method of conducting time-domain and frequency analysis of the transient waveform of the boost input current to identify fault types, the scheme proposed in this section is suitable for engineering applications. It only uses the comprehensive variation of the boost input voltage-current

TABLE I
SUMMARY OF THE BOOST PORT CHARACTERISTICS UNDER PV BUS ARC FAULTS

Fault type		Features of the boost input port		
		Voltage	Current	Control
Series arc	Situation 1	Decrease	Remain	Adjust MPPT
	Situation 2	Decrease	Decrease	Adjust MPPT
	Situation 3	No	No	Stop
Parallel arc	Situation 4	Remain	Decrease	Adjust MPPT
	Situation 5	Decrease	Approach 0	Arc extinguish
	Situation 6	Decrease	Approach 0	Arc extinguish

at the 10^1–10^2 ms level as the standard for fault identification and classification, and the implementation process is relatively simple. Since the time scale in the information extraction and feature analysis of the input current-voltage of the boost converter is at the 10^1–10^2 ms level, the influence of light and temperature changes in the environment on the PV output characteristics can be ignored at this time scale.

The characteristics of the boost input port when the series arc and parallel arc of the PV busbar occur analyzed in Sections III and IV are summarized in Table I. From the summary results, it can be known that when six types of arc faults occur, the voltage-current combination characteristics of the input port of boost are all different under the premise of maintaining MPPT control. Therefore, this combined feature can be utilized for arc fault identification and classification.

Based on the characteristics of the boost input ports and control modes summarized in Table I under various conditions of series/parallel arcs, the arc fault identification and classification design of PV busbar is carried out. The logical flow is shown in Fig. 14. The criteria for fault classification are directly related to the constraint characteristics of the arc on PV-boost. Therefore, after classifying the arc based on the differences of features, differential control of boost can be carried out through the detection results. That is, in the category of arc faults with relatively weak hazards, after identification, control and adjustment can be made through boost to maintain normal power generation operation, and enter the parallel operation mode of PV power generation and arc fault waiting for handling. In the category of arcs with stronger hazards, after the system detects them, rapid arc extinguishing treatment is required to ensure the safety of the system.

B. Design for Practical Application

In real-time arc detection, the use of sliding window overlapping sampling can enhance the detection frequency and the real-time performance of fault detection [30]. To fully detect the instantaneous changes in the arc, when using sliding window overlapping sampling, the relationship between a single control period T_1 and the data sampling period T_2 can be expressed as

$$1.5T_1 \leqslant T_2 < 2T_1 \tag{23}$$

The sliding window processing of sampling data is shown in Fig. 15. During each control cycle, about half of the time windows T_1 (blue timeline) have overlapping sampling data (red timeline). The sliding window processing can reflect the changes of time-domain features relatively completely, and can avoid the problem of incomplete sampling information caused by important information appearing at the edge position in traditional sampling method.

When a series arc fault occurs, the fault current signal has certain randomness and may contain high-frequency signals of different intensities. There is a significant switching noise at the switching frequency and its multiples of the inverter, as well as some large-amplitude random noise. If this noise is not removed, the arc characteristics will not be obvious, making it difficult to distinguish between normal and fault states. Therefore, it is necessary to average the time-domain signals of a single control cycle.

The fault identification algorithm based on the PV-arc-boost unified model proposed in this paper is shown in Fig. 14. Its arc fault detection method is determined jointly by the changes in the boost input voltage and current. The judgment rules for the fault are as follows:

$$V_{t-1} - V_t > \Delta V \tag{24}$$

$$I_{t-1} - I_t > \Delta I \tag{25}$$

Among them, for the series arc situation1 and situation 2, as well as parallel arc situation 4, the amplitude of voltage and current changes are relatively smaller compared to the remaining three arc faults. Therefore, a smaller set of thresholds (ΔV_1 and ΔI_1) is first set as the test standard for the above three types of arc faults. On the basis of this detection result, if the difference between the two sampling data exceeds the larger two thresholds (ΔV_2 and ΔI_2), it can be used as the judgment basis for series arc situation 3, parallel arc situations 5 and 6. The determination of these two sets of thresholds mentioned above is closely related to the parasitic inductance of the cable.

As shown in Fig. 16, there is a line inductance between the PV panel and the boost. When a series arc fault occurs, I_{in} decreases, and an induced voltage will be generated according to (26), where V_L is the induced voltage of PV module, and L is the inductance value. This induced voltage is included in the (27) of V_{in}.

$$V_L = L\frac{\mathrm{d}i}{\mathrm{d}t} \tag{26}$$

$$V_{\text{in}} = V_{\text{pv}} - v_{\text{gap}} + V_L \tag{27}$$

If an arc fault occurs, according to (24), V_{in} should drop by more than ΔV before it can be detected. However, the induced voltage (V_L) generated by the reduced current may counteract this voltage drop, thereby possibly hindering the detection of the arc fault.

According to the UL 1699B standard, an arc fault must be

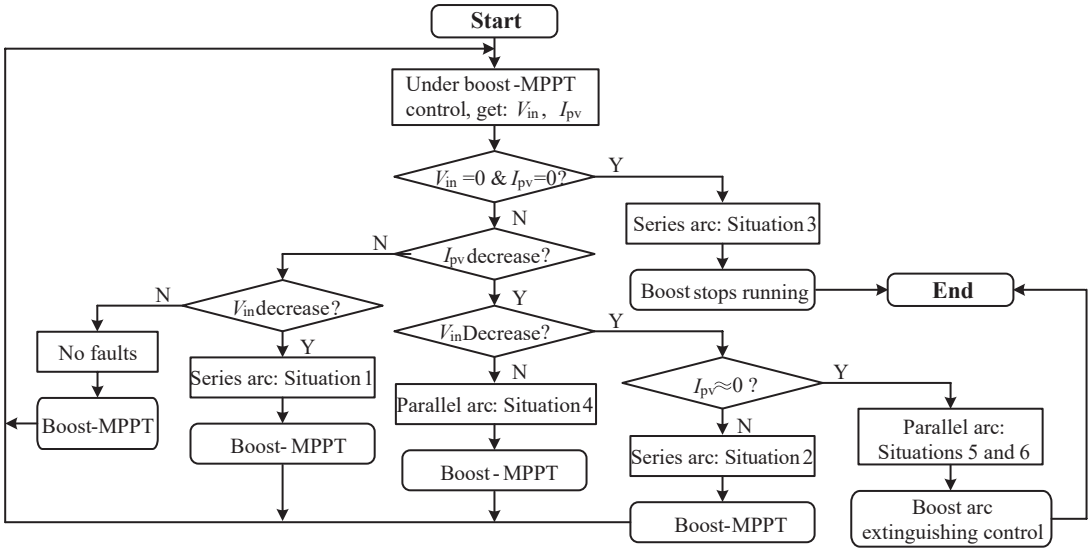

Fig. 14. Logic diagram for arc fault identification and classification of PV bus.

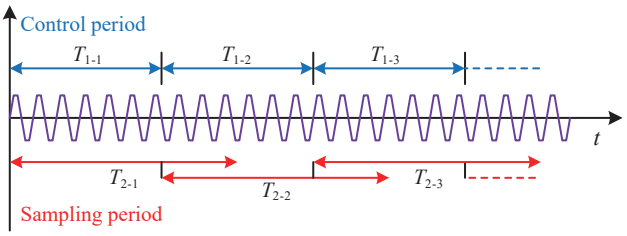

Fig. 15. Sliding window processing of sampled data.

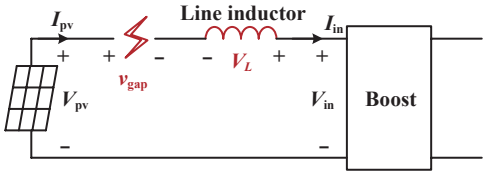

Fig. 16. Diagram of line inductor between PV and boost.

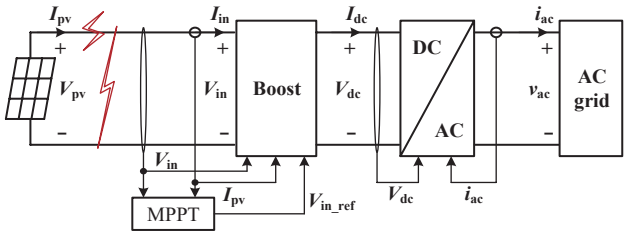

Fig. 17. The simulation platform and its control diagram.

detected within 2.5 s. This is one of the key requirements for ensuring system safety. To meet this safety requirement, in practical applications, it is necessary to first determine whether the line inductance between PV panel and the boost converter will affect the detection effect, and then further determine the threshold ΔV to avoid interference with the arc fault detection.

VI. Simulation and Experimental Verification

To further verify the effectiveness of the proposed equivalent model of the PV-boost power generation system based on series/parallel arc constraints and the arc fault type identification method, a simulation model as shown in Fig. 17 was built in this section for verification.

The boost conversion stage adopts the input voltage outer loop and inductor current inner loop control based on MPPT. The output side of boost is a voltage-type load, and its output bus voltage is controlled by the grid-connected inverter of the second stage. The specific parameters of the simulation model are shown in Table II.

TABLE II
Simulation and Experimental Parameters

	Parameters	Simulation	Experiment
PV	Maximum power P_{mppt} / W	7800	650
	MPP voltage V_{mppt} / V	423.6	70.5
	MPP current i_{pv_mppt} / A	18.4	9.2
Boost	Filter inductor L / μH	1200	220
	Input capacitance C_{in} / μF	47	33
	Output capacitance C_o / μF	330	110
	Switching frequency f / kHz	20	20
	Output bus voltage V_{dc} / V	750	115

A. Simulation Results

As shown in Fig. 18, it is the simulation result of the situation 1 of series arc. In this case, the arc current transmission capacity is greater than the MPPT current of the PV cell. Therefore, when the arc occurs, the MPPT regulation at the boost stage can bring the PV cell back to the maximum power output state. The voltage drop generated by the arc and the line current work together to form the loss link of the series arc. Therefore, when the steady-state current of MPPT remains

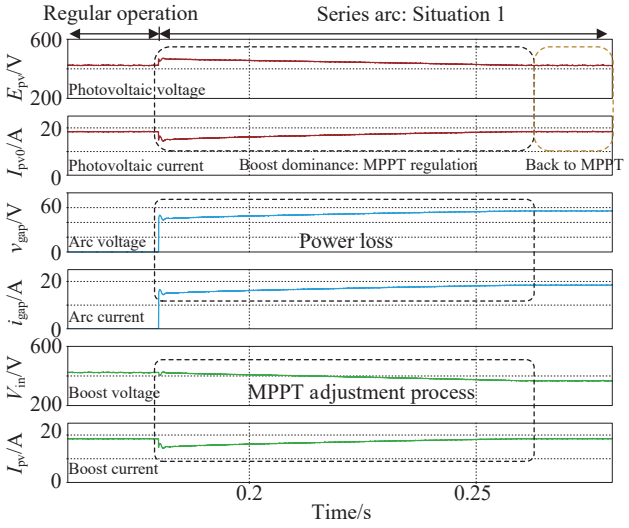

Fig. 18. Simulation results of series arc-situation 1.

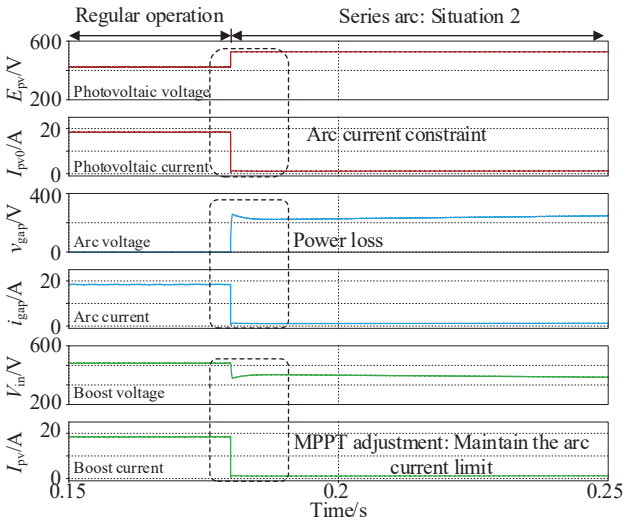

Fig. 19. Simulation results of series arc-situation 2.

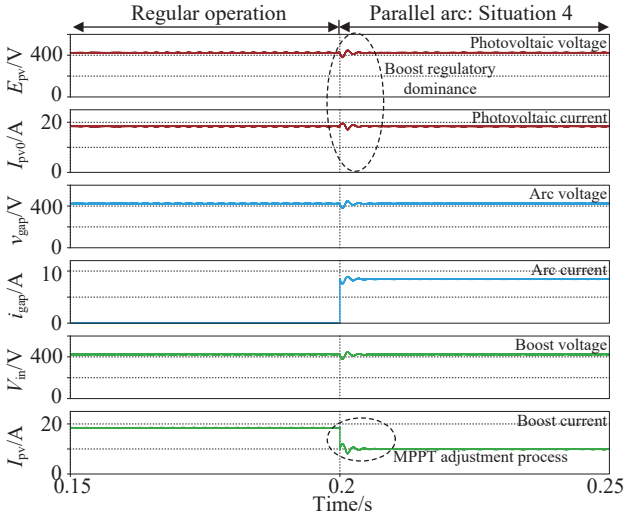

Fig. 20. Simulation results of parallel arc-situation 4.

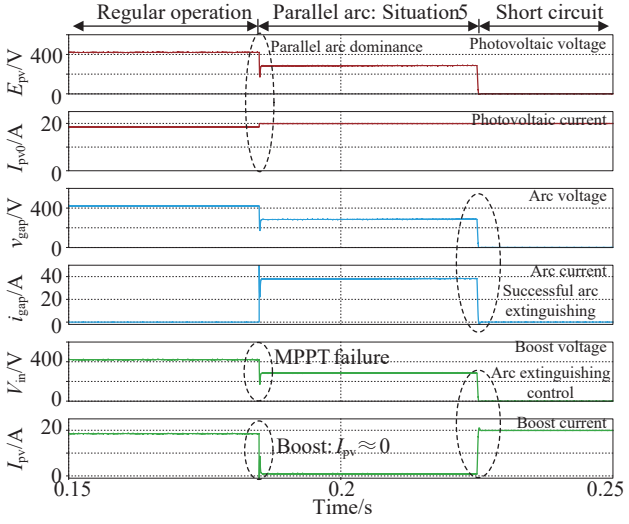

Fig. 21. Simulation results of parallel arc-situation 5 and its extinguishing control.

unchanged, the input voltage of the boost input stage drops. This voltage-current characteristic can be used as the judgment condition for the series arc-situation 1.

As shown in Fig. 19, it is the simulation result of the series arc-situations 2. In this case, the current-carrying capacity of the arc is lower than the MPPT current of the PV cell, thus limiting the current output capacity of the PV cell and causing it to no longer operate at the maximum power point. In this situation, when boost performs MPPT control, it will keep the input current at the arc current-carrying limit value to ensure that the PV cell can generate electricity at the maximum output power. At this point, both the input voltage and input current of boost will decrease. This feature can be used as a judgment condition for the series arc-situation 2. When the series arc-situation 3 occurs, the boost input bus is equivalent to an open circuit state, with both voltage and current being zero. Therefore, no further simulation verification is required for this situation.

As shown in Fig. 20, it is the simulation result of the parallel arc-situation 4. In this case, the current-carrying capacity of the parallel arc is lower than the output current at the maximum power point of the PV cell. Under the MPPT control of boost, PV cells can generate electricity at maximum power, and a portion of the power can be sent out through boost. The power loss of the parallel arc depends on the current-carrying capacity of the arc. In this case, the input voltage of the boost stage remains unchanged while the input current decreases. This feature can be used as the determination condition for parallel arc-situation 4.

The simulation results of parallel arc-situations 5 and 6 are shown in Figs. 21 and 22, respectively. In both cases, the current-carrying capacity of the parallel arc is higher than the output current at the maximum power point of the PV cell. When the above two types of faults occur, the PV bus voltage can no longer be maintained by boost control and is instead dominated by the arc. The power of PV power generation is basically consumed by electric arcs, and the current transmitted

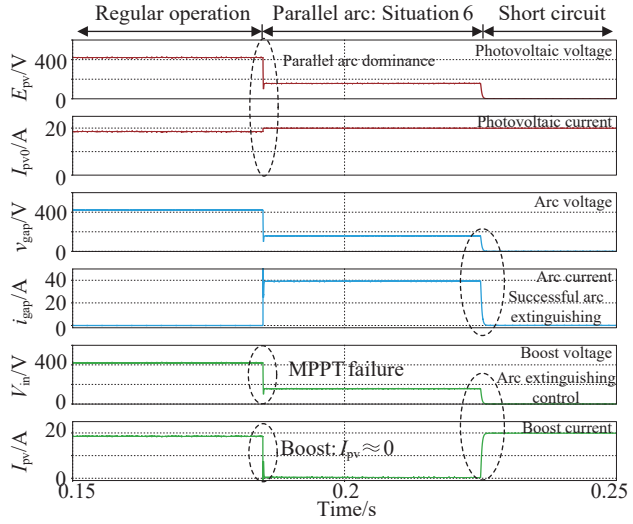

Fig. 22. Simulation results of parallel arc-situation 6 and its extinguishing control.

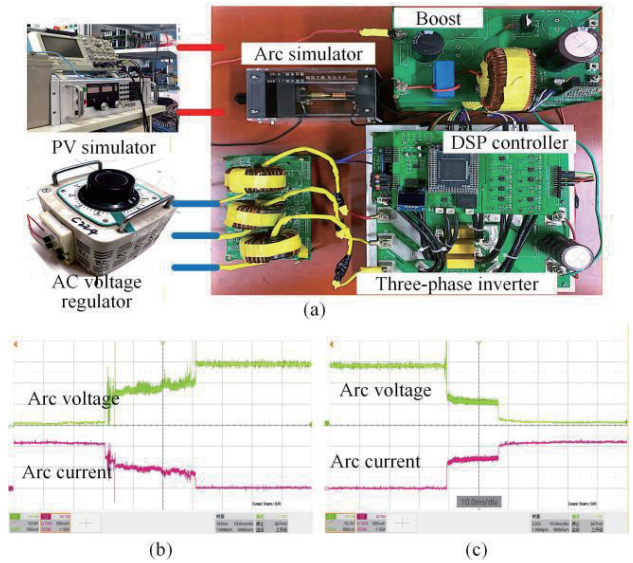

Fig. 23. Test results of the arc generation process. (a) Arc fault test experimental platform, (b) The process of closed-circuit, arc-initiation and arc-extinction, (c) The process of open-circuit, arc-initiation and closed-circuit.

by boost is close to zero. The above boost input voltage and current characteristics can be used as the conditions for judging these two types of arc faults. Moreover, under these two types of faults, the arc energy is relatively high and the arc burning is more intense. Therefore, the short circuit operation of the PV cell can be controlled by boost to rapidly reduce the arc voltage to zero, achieving the arc extinguishing effect.

B. Experimental Results

To further verify the effectiveness of the proposed equivalent model and identification method of the system under arc fault constraints, the paper established an experimental platform as shown in Fig. 23(a). Its framework structure and control method are shown in Fig. 17, and its parameters are listed in

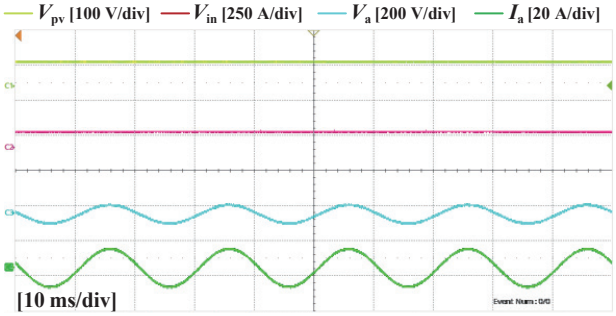

Fig. 24. Experimental results of each port under normal operation.

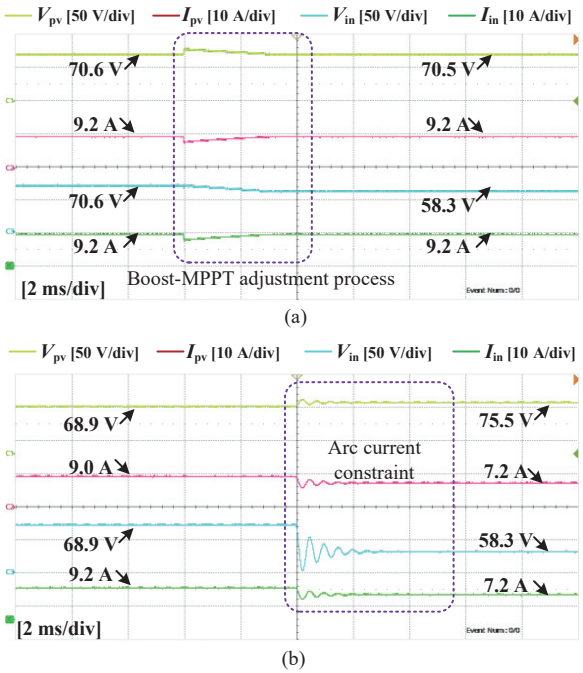

Fig. 25. Experimental results of (a) series arc-situation 1, and (b) series arc-situation 2.

Table II. The test waveforms of the arc process are shown in Fig. 23(b) and (c). The arc fault experiments in this section all adopt the method of switching to the arc faulty circuit when operating in the conventional mode. The characteristics of the arc branch are set after pre-testing.

1) Conventional Operating Condition Tests

Fig. 24 shows the waveforms of each port when the PV power generation system is operating in the MPPT state. At this time, the boost input voltage, that is, the maximum power point voltage of the PV is 70.5 V, the DC bus voltage of the inverter is 115 V, the voltage amplitude of the grid voltage regulator is 47 V, and the amplitude of the grid-connected current is 8.7 A.

Fig. 25 shows the experimental results of the series arc-situations 1 and 2. Fig. 25(a) shows the test waveform of the series arc-situation 1. When the PV busbar cuts into the series arc fault, the PV cell returns to the maximum power point output state after boost regulation. Before and after the series arc occurs, the boost input current remains constant while the

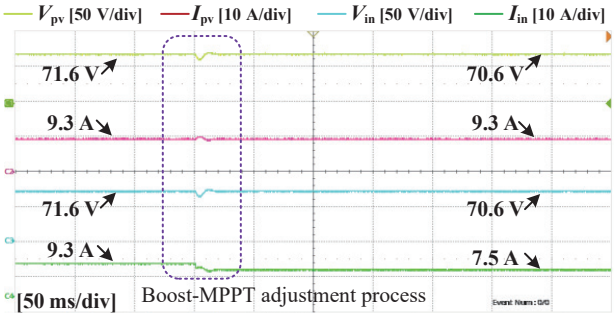

Fig. 26. Experimental results of parallel arc-situation 4.

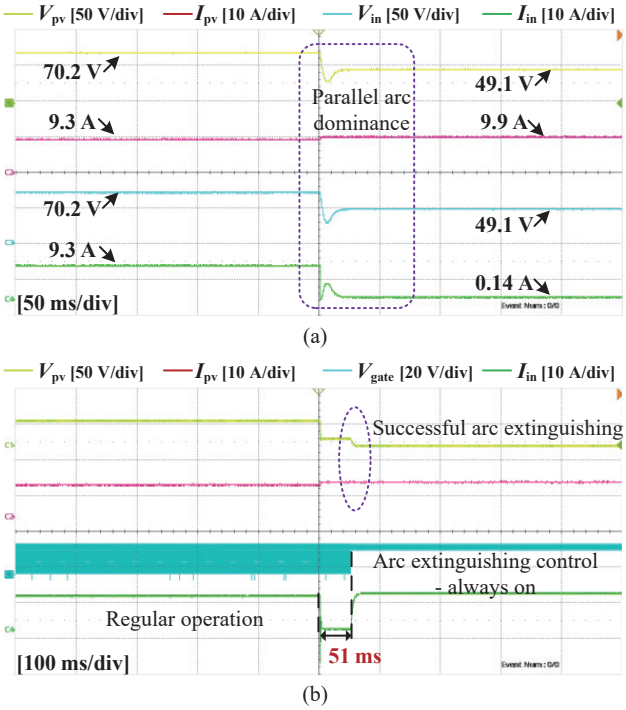

Fig. 27. Experimental results of parallel arc-situation 5. (a) Parallel arc-situation 5: phenomenon, (b) Parallel arc-situation 5: extinguishing control.

input voltage drops. The difference between the PV power and the boost input power is 112.2 W, which is the arc loss power. Fig. 25(b) shows the test waveforms of the series arc-situation 2. Constrained by the current-carrying capacity of the arc, the PV power generation current decreases, and its output voltage slightly increases, which is consistent with the external characteristics of the PV cell. The abandoned power of the PV cell is 76.5 W. Both the boost input voltage and current drop. After a series arc fault occurs, the difference between the PV power and the Boost input power is 400.5 W, which is the arc loss power.

Fig. 26 shows the experimental results of the parallel arc-situation 4, in which the preset arc current-carrying capacity is relatively low. When a parallel arc occurs, the boost input power decreases, and a portion of the power enters the arc branch, resulting in power loss, approximately 140.1 W.

Figs. 27 and 28 show the experimental test results of the more severe parallel arc scenarios, namely situations 5 and 6. When

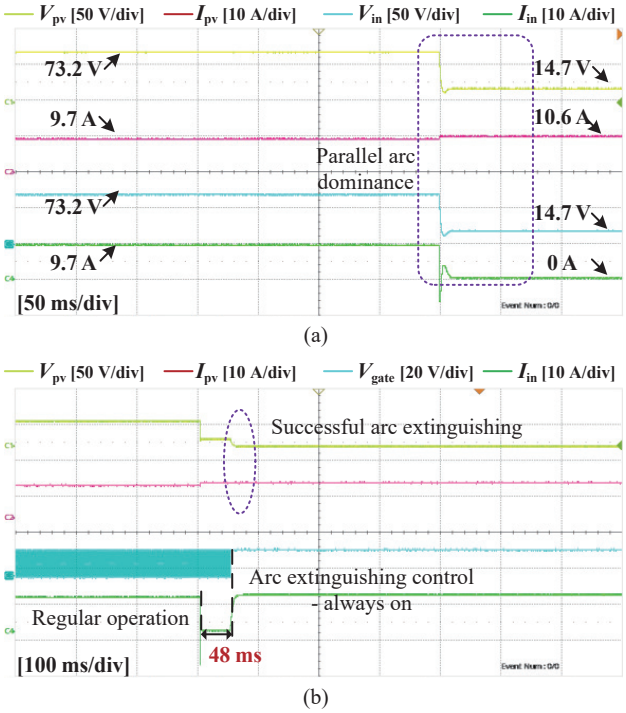

Fig. 28. Experimental results of parallel arc-situation 6. (a) Parallel arc-situation 6: phenomenon, (b) Parallel arc-situation 6: extinguishing control.

situation 5 occurs, if no protective measures are taken, the PV bus voltage will be dominated by the parallel arc and decrease, and the boost input current will be almost zero, indicating that the PV power generation is basically consumed by the arc. In this situation, the parallel arc, due to its higher energy, generates more intense combustion, and the harm is even more severe when situation 6 occurs. Therefore, both of the above situations require the design of arc-extinguishing schemes, as shown in Figs. 27(b) and 28(b). Approximately 50 ms after the fault occurs, the system detects the fault and takes arc-extinguishing measures, keeping the boost switch tube constantly on and short-circuiting the PV cell to zero voltage to achieve the arc-extinguishing control of the parallel arc.

2) Variable Operating Condition Tests

To further test the effectiveness of the fault classification and identification methods proposed in this paper, various operating conditions were tested in this section, including port changes (PV environment, AC grid), and the influence of different application scenarios (different cable lengths) on the detection algorithm.

Fig. 29 shows the test results of PV simulator setting the variation of intensity of solar radiation. Under the fault detection algorithm as shown in Fig. 14, regardless of whether the external environment's intensity of solar radiation increases or decreases, the changes in boost input voltage and current do not conflict with the detection characteristics of arc occurrence, and thus no false alarm phenomenon occurs.

Fig. 30 shows the test results when the grid voltage undergoes a transient change. As shown in Fig. 17, the AC grid is

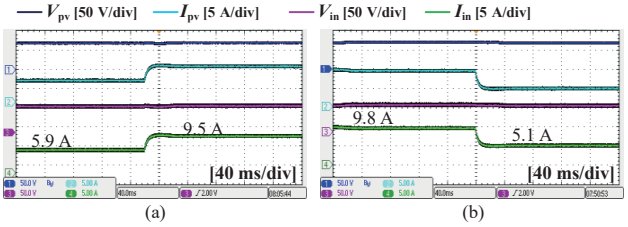

Fig. 29. Test waveforms of intensity of solar radiation variation. (a) Intensity of solar radiation increasing, (b) Intensity of solar radiation decreasing.

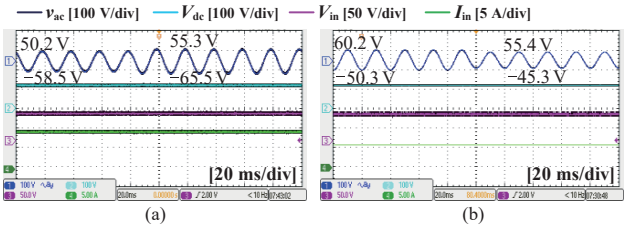

Fig. 30. Test waveforms of grid voltage variation. (a) Grid voltage rising, (b) Grid voltage falling.

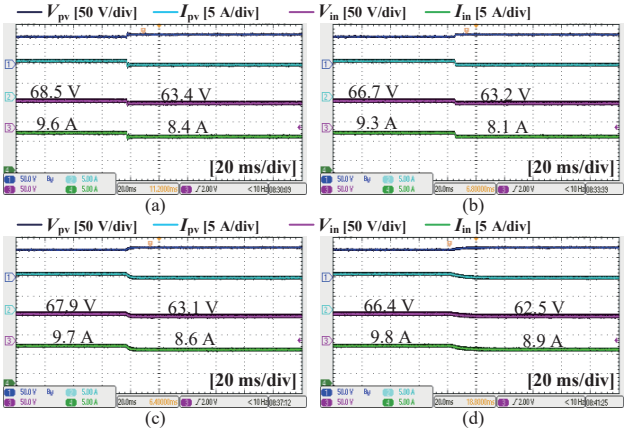

Fig. 31. Test waveforms under different cable lengths. Cables with lengths of (a) 1 m, (b) 2 m, (c) 10 m, and (d) 30 m.

separated from PV bus by two-stage converters, namely three-phase inverter and boost converter. The inverter adopts DC bus voltage control, and can maintain V_{dc} stability when the grid voltage changes. The boost converter maintains its input voltage stability under MPPT control. Therefore, under the control and buffering of the two-stage converters, whether the grid voltage rises or falls, it will not affect the boost input voltage and current, nor will it affect the arc fault detection algorithm.

As shown in Fig. 31, for the case of series arc condition 2, the test results of arc occurrence under different cable lengths between the PV panel and the boost converter are presented. According to the analysis in Section V.B, the parasitic inductance of the circuit varies with different cable lengths, and thus the changes in the input voltage and current of the boost are also different. Therefore, in practical applications, it is necessary to pay special attention to the influence of the parasitic inductance introduced by different cable lengths. In the experiment, based on the voltage and current change rates determined by different cable lengths, different arc fault detection thresholds are set, which can maintain the PV power control based on arc current constraints in the series arc condition 2.

VII. Conclusions

This paper aims at the series/parallel arc problem existing in the intermediate busbar between PV cell and boost converter, and proposes a unified model of PV-boost power generation system based on series/parallel arc constraints and specific faults identification and classification methods. Based on the basic models of PV cells and arcs, the output external characteristics of the PV system in fault state were analyzed. By establishing a unified model of PV-arc-boost, the operating mechanism and power transfer characteristics of the system under two types of arc faults were revealed. Based on the above analysis conclusions, a specific faults identification and classification scheme for series/parallel arcs based on the degree of hazard was designed. Its feasibility has been effectively verified.

References

[1] J. Teng, X. Sun, X. Liu, W. Zhao, and X. Li, "Power mismatches elimination strategy for MMC-based photovoltaic system and lightweight design," in *IEEE Transactions on Power Electronics*, vol. 38, no. 9, pp. 11614–11629, Sept. 2023.

[2] J. Teng, X. Liu, Z. Wang, L. Qi, M. Zhang, W. Zhao, X. Li, and X. Sun, "A novel CHB-based photovoltaic grid-tied system integration of centralized energy storage and its power security domain," in *IEEE Transactions on Circuits and Systems I: Regular Papers*, vol. 71, no. 10, pp. 4837–4850, Oct. 2024.

[3] Y. Pang, H. Yang, Y. Ji, X. Zhang, Y. Zhu, G. Li, Z. Xiang, C. Gong, S. Qiu, H. Zhou, M.-C. Wong, and J. Lin, "A multiple energy conversion channels fusion grid-connected inverter for large-scale PV active power injection preventing power loss caused by insufficient MPP PV voltage," in *IEEE Transactions on Power Electronics*, vol. 40, no. 9, pp. 13415–13433, Sept. 2025.

[4] G. Ding, F. Gao, H. Tian, C. Ma, M. Chen, G. He, and Y. Liu, "Adaptive DC-link voltage control of two-stage photovoltaic inverter during low voltage ride-through operation," in *IEEE Transactions on Power Electronics*, vol. 31, no. 6, pp. 4182–4194, Jun. 2016.

[5] Z. Yin, S. Peng, C. Xiao, L. Wang, and S. Yang, "A series arc fault detection method based on time-frequency Markov permutation transition field for photovoltaic systems with power electronic devices," in *IEEE Transactions on Power Electronics*, vol. 40, no. 8, pp. 11380–11393, Aug. 2025.

[6] M. Z. T. Nashrulloh, E. Prasetyono, and D. O. Anggriawan, "Mapping detection of DC series arc fault based on fast Fourier transform" in *International Electronics Symposium (IES)*, pp. 582–587, 2021.

[7] C. He, L. Mu, and Y. Wang, "The detection of parallel arc fault in photovoltaic systems based on a mixed criterion," in *IEEE Journal of Photovoltaics*, vol. 7, no. 6, pp. 1717–1724, Nov. 2017.

[8] C. Wu, Y. Zheng, F. Wang, and Z. Li, "Simulation study on the impact of microgrids on DC arc," in *Proceedings of 2020 5th International Conference on Power and Renewable Energy (ICPRE)*, Shanghai, China, 2020, pp. 272–277.

[9] H. Wang, X. Wang, T. Fan, J. Wang, Z. Lin, Y. Shen, J. Su, and P. Zhang, "DC series arc fault detection method in photovoltaic system based on multiple frequency selections for common-mode conductive voltage," in *IEEE Transactions on Power Electronics*, vol. 37, no. 12, pp. 15538–15553, Dec. 2022.

[10] N. L. Georgijevic, M. V. Jankovic, S. Srdic, and Z. Radakovic, "The detection of series arc fault in photovoltaic systems based on the arc current entropy," in *IEEE Transactions on Power Electronics*, vol. 31, no. 8, pp. 5917–5930, Aug. 2016.
[11] W. Wang, A. C. F. Liu, H. S. H. Chung, R. W. H. Lau, J. Zhang, and A. W. L. Lo, "Fault diagnosis of photovoltaic panels using dynamic current-voltage characteristics," in *IEEE Transactions on Power Electronics*, vol. 31, no. 2, pp. 1588–1599, 2016.
[12] M. Jalil, H. Samet, T. Ghanbari, and M. Tajdinian, "Development of nottingham arc model for DC series arc modeling in photovoltaic panels," in *IEEE Transactions on Industrial Electronics*, vol. 69, no. 12, pp. 13647–13655, 2022.
[13] H. Zhao, Y. Chen, M. Tian, and X. Shi, "DC arc model superimposing current-controlled arc noise on a heuristic average model," in *IEEE Transactions on Aerospace and Electronic Systems*, vol. 60, no. 2, pp. 1260–1271, 2024.
[14] M. M. A.-H. Salim, and M. AlMuhaini, "DC arc flash modeling and analysis of photovoltaic arrays using magnetohydro dynamic framework," in *IEEE Transactions on Dielectrics and Electrical Insulation*, vol. 32, no. 2, pp. 641–648, Apr. 2025.
[15] W. Kim and H.-P. Park, "Design methodology of power-level modulation for PV power loss minimization and DC series arc fault detection and extinguishing," in *IEEE Access*, vol. 13, pp. 109057–109068, 2025.
[16] S. Chang, D. Cha, J. Choi, J.-H. Ahn, S.-G. Song, W. Kim, and H.-P. Park, "DC series arc fault detection capability with non-inverting buck-boost converter for module-level power electronics applications," in *IEEE Journal of Emerging and Selected Topics in Power Electronics*, vol. 13, no. 6, pp. 7489–7498, Dec. 2025.
[17] B. Kim, T. Kim, W. Kim, and H. -P. Park, "DC series arc fault detection and extinguishing with modulation algorithm of non-inverting buck-boost converter for PV applications," in *IEEE Access*, vol. 13, pp. 49504–49513, 2025.
[18] H. P. Park, S. J. Chang, J. Y. Park, M. Kim, W. Kim, and S. Chae, "DC series arc fault detection method with resonant filter design for PV systems," in *IEEE Transactions on Power Electronics*, vol. 39, no. 11, pp. 14240–14250, 2024.
[19] Z. Yin, L. Wang, B. Zhang, L. Meng, and Y. Zhang, "An integrated DC series arc fault detection method for different operating conditions, " in *IEEE Transactions on Industrial Electronics*, vol. 68, no. 12, pp. 12720–12729, 2021.
[20] H. Park and S. Chae, "DC series arc fault detection algorithm for distributed energy resources using arc fault impedance modeling, " in *IEEE Access*, vol. 8, pp. 179039–179046, 2020.
[21] W. Miao, F. Zhi, Q. Chen, T. Shi, and F. Wang, "Series arc fault detection by modeling and integral regulated residual analysis," in *IEEE Transactions on Consumer Electronics*, vol. 71, no. 1, pp. 1125–1135, 2025.
[22] W. Miao, Q. Chen, and F. Zhi, "Low-voltage DC-arc-current model by time-series interval prediction and equivalent circuit model," in *IEEE Transactions on Power Delivery*, vol. 40, no. 5, pp. 2840–2849, 2025.
[23] B. Kim, W. Kim, M. Jeon, S. G. Song, and H. P. Park, "Coordination of machine learning and current modulation for DC series arc fault detection and extinguishing for module-level PV systems," in *IEEE Transactions on Power Electronics*, vol. 40, no. 11, pp. 16061–16067, 2025.
[24] J. Yan, Q. Li, and S. Duan, "A simplified current feature extraction and deployment method for DC series arc fault detection," in *IEEE Transactions on Industrial Electronics*, vol. 71, no. 1, pp. 625–634, 2024.
[25] K. C. Paul, D. Waldmann, C. Chen, Y. Wang, and T. Zhao, "Artificial intelligence for DC arc fault detection in photovoltaic systems: A comprehensive review," in *IEEE Access*, vol. 13, no. Apr., pp. 90766–90794, 2025.
[26] Y. Mao, S. Safa, G. Smith, L. Wurth, R. Weiss, and J. Hagemeyer, "Why AI: A comparative study for detection methods in DC series arc fault," in *IEEE Access*, vol. 13, no. Feb., pp. 42703–42722, 2025.
[27] W. Kim, Y.-J. Kim, and H. Kim, "Arc voltage and current characteristics in low-voltage direct current," in *Energies*, vol.11, no.10, p. 2511, 2018.
[28] W. Miao, Q. Chen, and F. Zhi, "Low-voltage DC-arc-current model by time-series interval prediction and equivalent circuit model," in *IEEE Transactions on Power Delivery*, vol.40, no.5, pp.2840–2849, 2025.
[29] W. Wang, A. C. F. Liu, H. S. H. Chung, R. W. H. Lau, J. Zhang, and A. W. L. Lo, "Fault diagnosis of photovoltaic panels using dynamic current-voltage characteristics," in *IEEE Transactions on Power Electronics*, vol. 31, no. 2, pp. 1588–1599, 2016.
[30] S. Grosche, A. Regensky, J. Seiler, and A. Kaup, "Boosting compressed sensing using local measurements and sliding window reconstruction," in *IEEE Transactions on Image Processing*, vol. 29, pp. 7931–7944, 2020.

Kailong Chen received the B.S. and M.S. degrees in electrical engineering in 2014 and 2017, respectively, from Yanshan University, Qinhuangdao, China, and is currently working toward the Ph.D. degree in electrical engineering with Yanshan University, Qinhuangdao, China.

He has been the Deputy Director of the New Energy and Energy Storage Research Institute at Guodian Nanjing Automation Co., Ltd. since 2021. His research interests include dc-dc converters, multiple-input converters, and grid-forming issues.

Jiaxun Teng received the B.S. degree in electrical engineering from Harbin Institute of Technology, Weihai, China, in 2017, and the M.S. degree in power electronics and power drives and the Ph.D. degree in artificial intelligence from Yanshan University, Qinhuangdao, China, in 2021 and 2025, respectively.

He was a Researcher with the Key Laboratory of Power Electronics for Energy Conservation and Motor Drive of Hebei Province since 2021. He has been a Lecturer with Yanshan University since 2025. He has authored/coauthored more than 30 transactions and journal papers since 2020. His current research interests include circuit topology, modulation and control of cascaded multilevel converter-based MV/HV systems, multi-bus multi-port energy router, medium-voltage motor drive, power electronics transformer and artificial intelligence applications.

Peiyi Li received a Bachelor's degree in electrical engineering and automation from Southeast University in 2010.

From 2015 to the present, employed at Guodian Nanjing Automation Co.,Ltd. specializing in renewable energy control research. Since 2010, he has published/co-authored over 10 international conference and journal papers. His research interests include dc-dc converters, multiple-input converters, and grid-forming issues.

Junjie Guo received the B.S. degree in electrical engineering from Yanshan University, Qinghuangdao, China, in 2024, and is currently working toward the M.S. degree in electrical engineering with Yanshan University, Qinhuangdao, China.

His current research interests include modular multilevel converter and common-mode voltage suppression.

Lei Qi received the B.S., M.S. and Ph.D degrees in electrical engineering in 2014, 2017 and 2023, respectively, from Yanshan University, Qinhuangdao, China.

He was a Lecturer with Yanshan University since 2017. His current research interests include the energy management, nanogrids, and stability analysis.

Xiaofeng Sun received the B.S. degree in electrical engineering from Northeast Heavy Machinery Institute, Heilongjiang, China, in 1993, and the M.S. and Ph.D. degrees in power electronics from Yanshan University, Qinhuangdao, China, in 1999 and 2005, respectively. From 2003 to 2007, he was an Associate Professor with Yanshan University, where he has been a Professor since 2008. He is also the Director with the Key Laboratory of Power Electronics for Energy Conservation and Motor Drive of Hebei Province. He has authored or coauthored more than 200 transactions and conference papers.

His research interests include dc–dc converters, multiple-input converters, hybrid electric vehicles, microgrids, and power quality control.